ARTICLES

Satellite Radar Interferometry for Monitoring Ice Sheet Motion: Application to an Antarctic Ice Stream

Richard M. Goldstein, Hermann Engelhardt, Barclay Kamb, Richard M. Frolich

Satellite radar interferometry (SRI) provides a sensitive means of monitoring the flow velocities and grounding-line positions of ice streams, which are indicators of response of the ice sheets to climatic change or internal instability. The detection limit is about 1.5 millimeters for vertical motions and about 4 millimeters for horizontal motions in the radar beam direction. The grounding line, detected by tidal motions where the ice goes afloat, can be mapped at a resolution of ~0.5 kilometer. The SRI velocities and grounding line of the Rutford Ice Stream, Antarctica, agree fairly well with earlier ground-based data. The combined use of SRI and other satellite methods is expected to provide data that will enhance the understanding of ice stream mechanics and help make possible the prediction of ice sheet behavior.

Polar ice sheets appear to respond in a complicated way to global climatic change and internal instabilities (*1, 2*). The response is seen in changes in ice surface configuration, ice flow velocity, and the position of the grounding line for marine ice sheets that go afloat at their periphery. Detection of significant changes in these parameters, if and as they develop, is needed (*3*). The technique of SRI can be used to determine ice flow velocity and also grounding-line position, which relates closely to the possibility of marine ice sheet disintegration with rapid retreat of the grounding line (*4*). We here apply SRI to the Rutford Ice Stream, Antarctica, which is one of a class of ice sheet flow features for which monitoring is particularly needed. In the light of these and other published results, we consider the prospects for satellite monitoring of ice sheet behavior in the near future.

The Antarctic ice streams (*5*) are fast-moving currents, 30 to 80 km wide and up to 500 km long, within the generally slow-moving ice sheet. Some reach flow speeds of ~800 m year^{-1}, ~100 times as fast as the adjacent ice sheet (*3, 5*). Because of the large ice flux that they carry, the ice streams make the major contribution (~90%) to outflow from the ice sheet; if they were to speed up or widen sufficiently, they could become the immediate cause of ice sheet collapse (*2, 6*). Monitoring their extent and motions is therefore of much importance in the assessment of ice sheet response and is also valuable to the search for the physical mechanism of ice stream motion (*5, 7*).

R. M. Goldstein is with the Jet Propulsion Laboratory, California Institute of Technology, Pasadena, CA 91109. H. Engelhardt and B. Kamb are with the Division of Geological and Planetary Sciences, California Institute of Technology, Pasadena, CA 91125. R. M. Frolich is with the British Antarctic Survey, Cambridge CB3 0ET, United Kingdom.

Satellite Radar Interferometry

Satellite-borne imaging synthetic aperture radar (SAR), such as that currently provided by the Earth Remote Sensing Satellite–1 (ERS-1) of the European Space Agency (ESA), presents the opportunity for measuring surface displacement fields interferometrically by use of the coherence of the radar beam (*8, 9*). If two side-looking radar observations of the same scene are made from satellite locations sufficiently close together (*10*), interference between the two resulting SAR images can be obtained by comparison of the phases of the synthesized signals making up the two images. The phase shift from image 1 to image 2 at each pixel can be displayed in an interferogram of the image pair (Fig. 1A), which is a plot of the phase shift (color-coded) as a function of position. The phase shift is a measure of the line-of-sight component of displacement of the ground surface point in relation to the spacecraft from the time of one image to the other. By line of sight, we mean the inclined ray followed by a radar pulse from the satellite to a scattering point on the ground. Half a wavelength of line-of-sight displacement (2.8 cm for the ERS-1 radar of wavelength 5.6 cm) produces a phase shift of 360°. Thus, the fringe pattern is a contour map of the line-of-sight displacement, with contour interval 2.8 cm. The zero of the phase shift is arbitrary, hence displacements are determined only relative to the displacement of a chosen reference point. The line-of-sight displacement resolution is 1.3 mm, on the basis of phase noise evaluated in areas of broad, widely spaced fringes, such as those in the southwest corner of Fig. 2. By comparison, the typical pixel size that limits the resolution in noninterferometric imaging methods for measuring ground displacement (*3, 11*) is ≳25 m.

In order to obtain an interferogram, the two SAR images must be registered. This is achieved by means of a correlation algorithm (*12*). The phase data are then averaged and condensed (*13*), and a correction is made to the phase shift at each pixel to remove the estimated phase shift that results from the slightly different positions of the spacecraft when the radar data for the two images were obtained. In principle, there is also a correction for surface topography, but for the nearly flat ice sheet surface, this is negligible.

Application to the Rutford Ice Stream

The Rutford Ice Stream (9) is advantageous for a test of the capabilities of SRI monitoring because it has been studied by surface observation (*14–17*). It is one of the main outlets of the West Antarctic ice sheet, draining an area of high snow accumulation around the Ellsworth Mountains and emptying into the head of the Ronne Ice Shelf (*14*) at 79.0°S, 77.5°W. The marginal shear zones (Fig. 1B) appear as bright bands in Fig. 1A because of radar scattering from numerous ice-air interfaces in these crevassed zones. Flow traces, highly elongated surface ridges and troughs believed to be parallel to ice flow, are faintly visible in parts of the marginal shear zones and on the Minnesota Glacier, which enters from the southwest. These features are also seen in satellite optical images (*14, 15, 18*).

The fringe pattern (Fig. 1A) contains the combined effects of ice flow motion and tidal action over the 6 days between the images, taken on 8 and 14 February 1992. In the ice stream north of the grounding line (Fig. 1B), the ice is grounded, and tidal action is absent. Because the ice flow is roughly opposite to the line-of-sight azimuth, flow displacements have an appreciable line-of-sight component. Thus, the fringe pattern can be interpreted as a contour map of flow velocity in which the color sequence blue-yellow-red-blue represents increasing velocity. On this basis, the velocity north of the grounding line is high and only slightly varying over a 22-km-wide central band of broad fringes (Fig. 1A), dropping off abruptly and rapidly into the marginal shear zones, where the fringes become very narrow and in large part unresolved. The steep velocity gradient ends rather abruptly at the outer edge of the marginal shear zones, where the fringes become broad again. This flow pattern agrees with that found by ground-based measurements on transverse line D of (*15*). A similar pattern is found in ice stream E in the Siple Coast region of Antarctica, except that the velocity fluctuations in the central band are more pronounced (*3*).

To obtain quantitative results, we converted the line-of-sight relative velocities to horizontal flow velocity values. A line-of-sight motion of 2.8 cm (one fringe) in 6.0 days corresponds to a flow velocity of $(2.8/6.0)\ (\cos\psi \sin\theta)^{-1}$ cm day^{-1}, where θ is the inclination from vertical of the line of sight and ψ is the angle between the horizontal flow vector and the x direction in Fig. 1. The inclination θ varies from 19.9° to 26.6° as we go from bottom to top in Fig. 1. In the ice stream at the top of Fig. 1, where $\psi \approx 24°$ as judged from the azimuthal trend of the margins as seen in the image at $x = 0$ (*19*), the velocity contour interval of the fringe pattern is thus 1.14 cm day^{-1}.

One can assign absolute velocity values to the contours by counting fringes from a reference point where the surface velocity can reasonably be assumed to be essentially zero, outside the ice stream. We made this assumption for a point at $(x, y) = (26, 3)$, alongside the bedrock of the Flowers Hills (*20*) (Fig. 1B). Fringes can be counted from that point along a path running generally southward to the Minnesota Glacier, eastward through the marginal shear zone, and then northward along the central band of the ice stream. From the reference point, we count a total of 148 fringes up to the fringe peak at (38, 25), and from the peak northward, we count back down 54 fringes to point (0, 13) in the middle of the ice stream at the top of Fig. 1A, for a net fringe count of 94 there. The corresponding flow velocity at (0, 13) is 94×1.14 cm day^{-1} = 390 m year^{-1}. The velocity is a time average over the 6-day period between images.

Because the fringes disappear in the marginal shear zones except near their edges, a special treatment was necessary to carry the fringe counting through the marginal zone east of Minnesota Glacier. A sub-area was treated by the interference search procedure (*12*) at higher spatial resolution (*21*). The resulting interferogram (Fig. 2) shows that extremely fine fringes can be resolved and counted through the marginal shear zone in this area. In other parts of the marginal shear zones, however, the high-resolution treatment was not successful (*22*).

The apparent flow velocities determined by SRI fringe counting with position-dependent θ along the near-centerline longitudinal profile from (0, 13) to (31, 42) (long-dashed line in Fig. 1B) were compared with ground-based velocity measurements made in 1978–80 and 1984–86 along

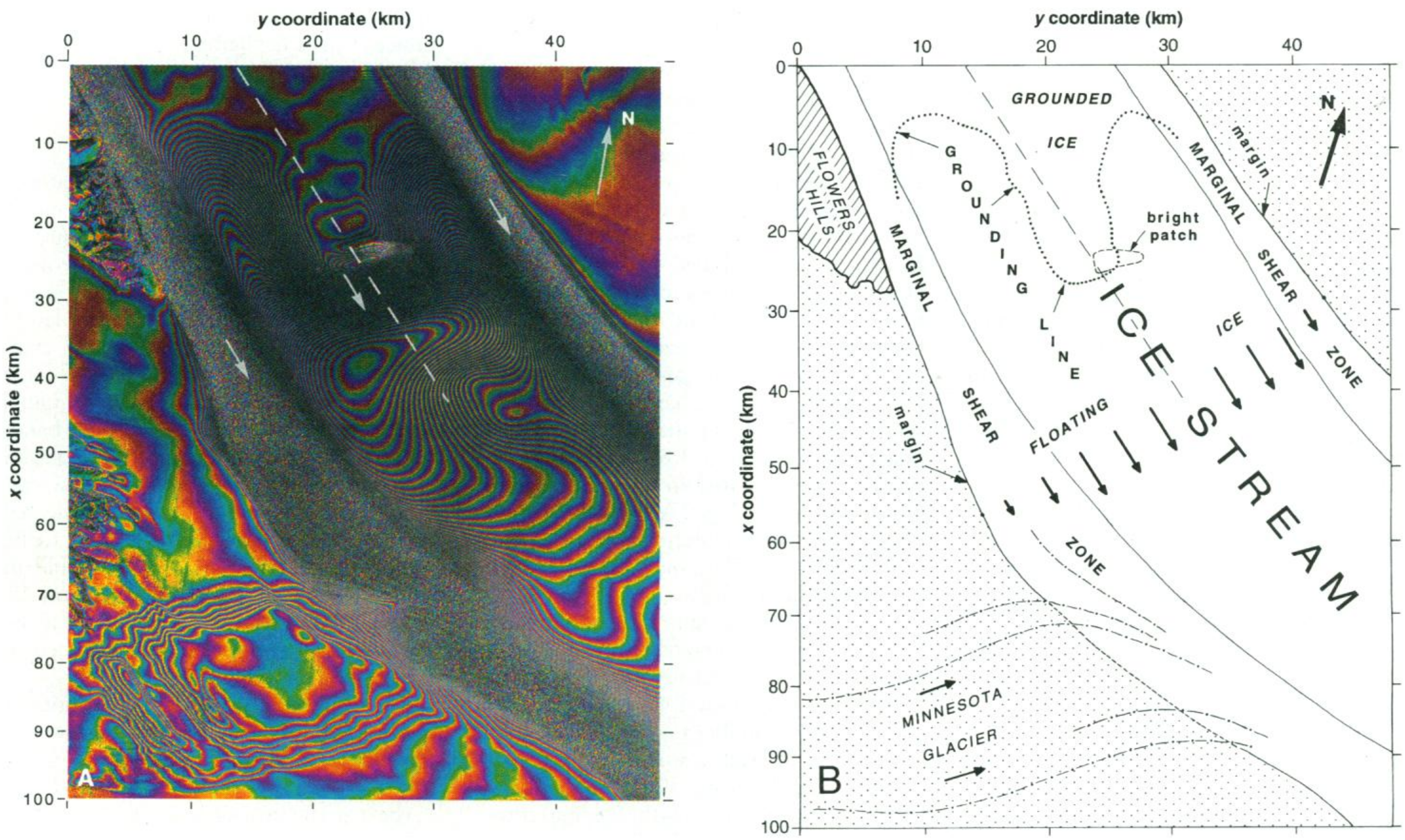

Fig. 1. (**A**) Radar interferogram of an area that includes a portion of the Rutford Ice Stream, Antarctica. Ice flow is indicated schematically by arrows. The center of the image is at 78°43′S, 83°0′W. The radar line-of-sight azimuth (350.8° true) is up. The color fringes show relative movement of the ice surface toward or away from the spacecraft during the 6-day period between two radar observations of the scene. Going from blue through yellow and red to blue again represents a 2.8-cm movement toward the spacecraft. The distance scales in the x and y directions are different, as shown by the marginal ticks. Superimposed on the interferogram is a radar amplitude image (conventional SAR image) of the same area, in shades of gray. (**B**) Location map for features in (A). The ice stream is the unpatterned area in the middle, flowing as indicated by arrows. The grounding line is shown dotted. Upstream from this line, the ice is grounded; downstream, it is afloat. Dash-dot lines show flow traces, faintly visible in (A). The long-dashed line running southeastward from (0, 13) is the centerline profile along which Fig. 3 is plotted. The corners of the image are located as follows: (0,0) at 78.30°S, 84.3°W; (100,0) at 79.19°S, 83.9°W; (0,49) at 78.25°S, 82.1°W; and (100,49) at 79.15°S, 81.7°W.

the same profile (Fig. 3) (*15*). From longitudinal coordinate 100 to about 124 km, the agreement is good, mostly within ±10 m year^{-1}. A similar degree of agreement is found between the transverse D profile of (*15*) and the SRI flow velocities along the top of Fig. 1A. Discrepancies could be caused by real changes in the time-averaged flow from 1978–80 and 1984–86 to 8 to 14 February 1992 or by various possible errors, both in the ground measurements and in the SRI, particularly in the choice of the off-stream reference point of zero velocity and in the value used for ψ.

Tidal Motion and Grounding Line

Downstream from longitudinal coordinate 128 km (Fig. 3), the apparent horizontal velocity obtained by SRI increases abruptly to a much higher level and persists with gradual decrease downstream from the peak at coordinate 139 km or at (38, 25) in Fig. 1A. These high apparent velocities are attributable to vertical motions where the ice stream is afloat and moves with the ocean tide. This interpretation is supported by comparison of the grounding-line pattern found by surface observations (*17*) with that indicated by Fig. 1A, in which the grounding line is the boundary between the area of broad fringes to the north (upstream) and narrow, closely spaced fringes to the south, corresponding to the abrupt increase in apparent velocity (Fig. 3). The comparison (Fig. 4) shows a considerable degree of agreement.

We found the vertical displacement needed to account for the fringe pattern downstream from longitudinal coordinate 128 km on the assumption that the contribution of the horizontal velocity to the line-of-sight displacement is given by the ground-based velocity measurements (Fig. 3). A maximum tidal uplift of about 2 m between the first and second radar observations is implied. This can be checked because the Fourier components for the observed tide near the Rutford Ice Stream have been evaluated (*17, 23*). Calculation on this basis (*24*) indicates that between the first and second observations there was a tidal rise of 2.1 ± 0.2 m.

The shape of the tidal uplift curve is compatible with the theory of ice shelf tidal flexure (Fig. 3). According to the standard bending–elastic-beam model of tidal flexure (*23*), the tidal uplift curve $\Delta z(x)$ has the form

$$\Delta z(x) = \Delta z_\infty \left[1 - e^{-\beta x}\sqrt{2}\,\sin\left(\beta x + \frac{\pi}{4}\right)\right] \quad (1)$$

Here, $\Delta z(x)$ is the change in elevation of the ice surface at x when the far-field tidal rise from observation 1 to observation 2 is Δz_∞, x is distance downstream from the grounding line (*25*), and β is a parameter that depends on the ice thickness and elastic modulus. The curve calculated from Eq. 1 with $\Delta z_\infty = 2.07$ m and with $\beta = 0.26$ km^{-1}, which is close to the preferred model value 0.25 km^{-1} (*23*), is in good agreement with the observed values (Fig. 3). This agreement supports the tidal uplift interpretation (*26*).

The progressive decrease in fringe count along the central band of broad fringes that extends downstream from (38, 25) in Fig. 1A is probably attributable to downstream decrease in both the tidal amplitude and the flow velocity of the ice stream. Other details in the fringe pattern, such as the curious indentations near (71, 26) and (44, 38), appear to be related to local grounding downstream from the main grounding line (*14*). The small peak at 126 km in the SRI velocity curve (Fig. 3) and the small minimum at 128 km appear to reflect the vertical component of grounded-ice motion over an ice-surface hump that is visible in Landsat images (*14, 15, 18*) near 78°29.7′S, 83°05′W. The bright patch at (24, 25), which comes from the SAR amplitude image, is probably attributable to crevassing of the ice as it flows over the hump.

It suggests that the grounding line retreated about 2 km between 1980 and 1992. However, this conclusion is uncertain because of uncertainties in registration be-

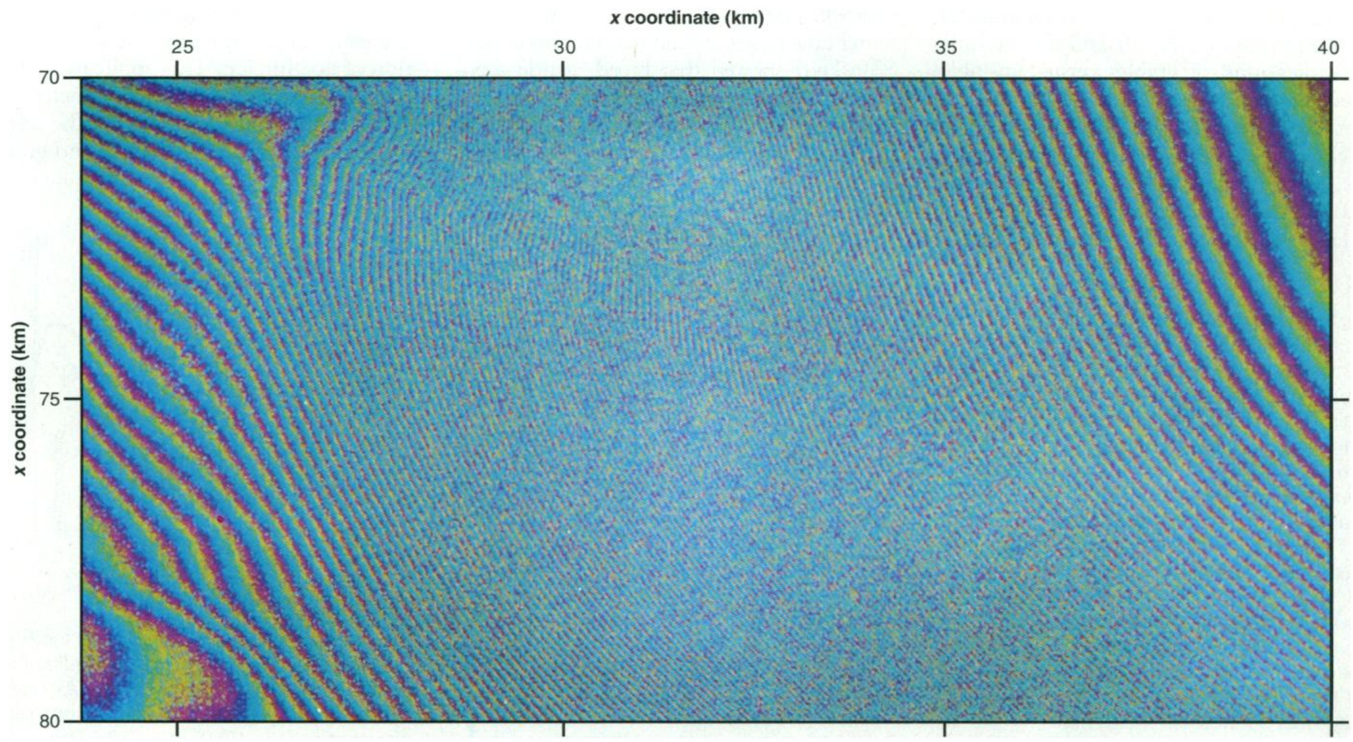

Fig. 2. Enlargement of a portion of Fig. 1 in the area where the Minnesota Glacier feeds into the Rutford Ice Stream. The radar amplitude (SAR) image is omitted, so that only the phase shift between the two complex images is portrayed. For greater spatial resolution of the fringes, the data averaging procedure (*13*) has been modified (*21, 22*).

tween the SAR image and the ground-based map (*27*).

Prospects for Satellite Monitoring of Ice Sheets

The foregoing results provide a basis for assessment of the potential role of SRI together with two already established satellite techniques for monitoring the ice sheets: satellite sequential imaging (SSI), which is used to measure ice flow velocity, and satellite radar altimetry (SRA), used to measure the configuration of the ice surface. Using downward-looking optical images, SSI tracks in map view the motion of crevasses and other surface features resolvable at the pixel scale or greater (*3*). Images from SAR can also be used, but with restrictions associated with the side-looking radar geometry. With the use of downward-directed radar pulses, SRA obtains a profile of ice sheet surface elevation along the satellite orbital track (*28*). The three techniques are so new that there is not yet a substantial body of results to consider, but we indicate our expectations for the near future.

For ice stream flow velocity monitoring, SRI and SSI are capable of comparable accuracy (~0.6 m year^{-1} for SRI, ~2 m year^{-1} for SSI) but over very different time scales—SRI over a time scale of a few days, SSI over 1 or 2 years (*29*). Well suited to obtaining the intermediate-term (~1 year) average flow and its changes over periods of several years, SSI will provide information needed in assessing the flow mechanism of the ice streams (*5, 7, 30*) and in watching for indications of stable versus unstable response to external climatic forcing or internal conditions. Of particular importance are changes in ice stream width and flux, which could indicate increased outflow and thus possibly the onset of ice sheet collapse (*2, 6*), and changes in the ice stream headwater regions, which could indicate the involvement of ice of the deep interior in such collapse. The same information can be provided more immediately by SRI, provided that certain conditions noted below are met.

The ability of SRI to obtain velocities in as short a time as 6 or even 3 days will allow it to observe short-term flow variations, which may prove to be important because the key to the ice stream mechanism (*7*) may lie in the relation of such changes in flow to changes in measured physical variables that can affect flow, such as basal water pressure. Also, SRI can get results under conditions of darkness or cloud cover, which is decidedly advantageous in obtaining short-term velocities.

For SSI, there is difficulty in getting optical images that are cloud-free and suitably illuminated. However, with an interval of ≳2 years between images (*29*), the chance of getting a pair of suitable images is not unacceptably low. A corresponding obstacle for SRI is getting interference between SAR images: Our success rate of one in three tries (at 6-day intervals) is some indication of the statistics involved but is not necessarily transferable to other parts of the ice sheets, where weather conditions that affect degradation of the interference (*29*) may be different.

Both SRI and SSI can detect only relative, rather than absolute, ice motions unless within the image there are fixed bedrock points or ice features that remain fixed with respect to bedrock. Bindschadler and Scambos (*3*) found how to get around this limitation with SSI: They showed that broad, gentle topographic undulations, made visible in optical [Landsat Thematic Mapper (TM)] images by faint sun shadowing or surface scattering-angle effects, remain fixed in position relative to the bedrock below and can be used as a surrogate bedrock reference to obtain absolute flow velocities. The hump on Rutford Ice Stream noted in the last section is probably an undulation of this type. For flow velocities from an SRI interferogram, there is no counterpart to the undulation reference for SSI. To obtain absolute flow velocities, SRI is dependent on an assumed surface reference point of zero or known velocity. The assumption of a reference point outside a fast-moving ice stream can involve an error only of the order of ice sheet flow velocities (≲10 m year^{-1}), which are small compared to ice stream velocities (~400 m year^{-1}). Hence, significant changes in ice stream flow can be monitored with useful accuracy by this method (*33*). The method does, however, require resolution of the very fine fringe pattern in marginal shear zones, which is difficult, as noted earlier (*22*).

The possible zero-velocity error could be eliminated if, within the area of a given SAR image, a marker is established whose motion is obtained on the ground, for example, by the Global Positioning System (GPS), which would provide a reference point of known velocity. The availability of a few widely spaced GPS reference points would open up the prospect of monitoring the flow of the ice sheets over broad areas outside of the ice streams as well as within them. For this, SRI would probably be needed because outside the ice streams, there is a general scarcity of the visible crevasses on which the SSI method depends.

The sensitivity of SRI (but not SSI) to vertical motions makes SRI highly suitable for locating the grounding line by detecting the effect of the tides on the surface elevation of floating ice. This application of SRI is not dependent on a zero-velocity reference because it is based only on the relative vertical motion of the floating and ground-

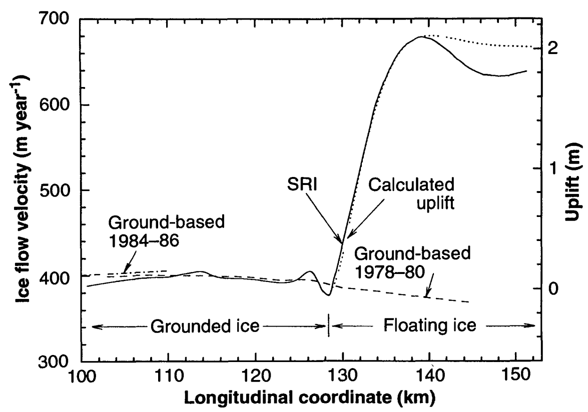

Fig. 3. Interpretation of ice stream motion along the longitudinal profile marked in Fig. 1. The abscissa is a longitudinal coordinate with origin 100 km upstream from the north end of the profile shown here (*15*). Where the ice is grounded, upstream (left) of coordinate 128, the solid curve gives the ice flow velocity (ordinate scale on left) obtained from the SRI data in Fig. 1A under the assumption that the phase shift results from horizontal motion (see text). The dashed and dash-dot lines give ground-based velocity measurements made in 1978 to 1980 and 1980 to 1984 (*15*). Downstream (right) of coordinate 128, where the ice is afloat, the solid curve gives the tidal uplift (ordinate scale on right) obtained from the SRI data on the assumption that the ice flow velocity is the same as the ground-based measurements. The dotted curve is calculated from the theory of tidal flexure, Eq. 1.

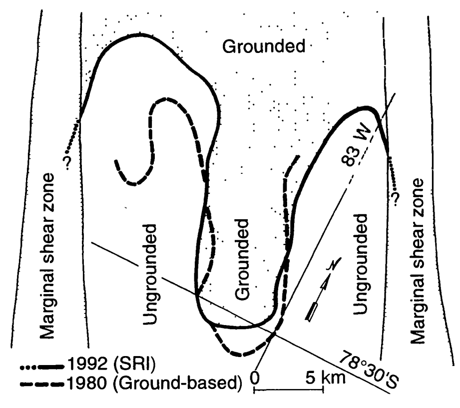

Fig. 4. Map of the grounding line of the Rutford Ice Stream: solid curve, grounding line as obtained from SRI in 1992 (Fig. 1A); dashed curve, grounding line as found from ground observations in 1980 (*17, 23*). The area of currently grounded ice is lightly stippled, and the marginal shear zones are more heavily stippled. Ice flow is from top to bottom.

ed ice. The prospect of being able to monitor grounding-line migration readily and systematically is of much importance in relation to the long-held concept that disintegration of the West Antarctic ice sheet can occur in an unstable manner tightly linked to retreat of the grounding line (*4*). Although SRA might seem to be a tool for this monitoring task also, the limitation to coverage along isolated satellite tracks rather than in a two-dimensional image is disadvantageous. Moreover, a radar-altimeter accuracy of ~1 m for single measurements (*28, 34*) makes SRA only marginally capable of detecting the tidal motion.

Monitoring of changes in grounding-line position from one SRI interferogram to another is probably not limited by the accuracy of grounding-line location in the fringe pattern (~0.5 km) but rather by the registry of the interferograms in relation to fixed bedrock. Analogously to what can be done with optical images (*3*), for this type of registry, a surrogate bedrock reference may be provided by features in the SAR image, such as the bright patch in Fig. 1A or the small peak and minimum in vertical motion associated with flow over a hump in the ice surface topography as noted earlier and seen in Fig. 3.

With the capability of monitoring long-term changes in ice surface elevation, SRA can follow the volumetric growth or shrinkage of an ice sheet. The one extensive program of this kind, applied to the southern half of the Greenland ice sheet, gave a growth in surface elevation of 0.23 ± 0.03 m year^{-1} (*28*). Because this is twice as great as the results of a ground-based survey (0.11 ± 0.03 m year^{-1}) and because the large error of individual elevation measurements required the averaging of a large number of SRA observations, the validity of the satellite result has been viewed as uncertain (*28*). Despite its high sensitivity to vertical motions, SRI is not applicable to this type of surface elevation monitoring. Laser altimetry of the ice sheet surface can now be done to an accuracy of about 0.4 m from aircraft (*35*), which makes it competitive with SRA for future satellite applications of this type.

The extensiveness of the results from ice sheet monitoring that can be expected in the near future from SRA, SSI, and SRI along the lines discussed above depends, of course, on the availability of satellites that can make these kinds of observations. Although ERS-1 carries both SRA and SAR [as well as infrared imaging capability in the Along-Track Sensing Radiometer (ATSR)], its orbit is only occasionally configured in the "ice mode" in which ice sheet SRI can be done (this mode has 43 orbital revolutions in exactly 3 days). The Japanese JERS-1 and the Canadian RADARSAT (to be launched in 1995) both have SRI capability; how much will be allocated to ice sheet SRI is not yet known, but RADARSAT is designed so that its side-looking radar can reach both the north and south poles with an appropriate change in spacecraft orientation. The best satellites for optical SSI are LandsatTM, the Japanese Marine Observation Satellite (MOS), and the French SPOT. The latter has the best spatial resolution (10 m), but its field of view is restrictively small. For a comprehensive summary of existing and potential satellite capabilities for ice sheet monitoring, see (*36*).

Our expectation is that wide-ranging satellite observations of ice motions and surface configuration as discussed above, together with local ground-based and airborne geophysical observations in key areas, will in a few years lead to a comprehensive mechanistic model of the West Antarctic ice sheet and its contained ice streams, on the basis of which predictions of its future behavior will be attempted [a first such attempt has already been made (*2*)]. Satellite monitoring of changes in the ice sheet if and as they develop will provide the information needed to judge whether the ice sheet is responding in a stable or unstable way to climatic change or other forcing. Ultimately such considerations will be applied also to the East Antarctic and Greenland ice sheets. The immediate focus on the West Antarctic ice sheet arises because of concern that it might collapse in the near future, leading to a significant rise of sea level (*37*).

REFERENCES AND NOTES

1. J. Oerlemans and C. J. van der Veen, Eds., *Ice Sheets and Climate* (Reidel, Dordrecht, Netherlands, 1984); R. B. Alley, *Episodes* **13**, 231 (1990); ______ and I. M. Whillans, *Science* **254**, 959 (1991); C. S. Lingle *et al., J. Geophys. Res.* **96**, 6849 (1991); T. J. Hughes, *Palaeogeogr. Palaeoclimatol. Palaeoecol.* **97**, 203 (1992); D. Sugden, *Nature* **359**, 775 (1992); S. S. Jacobs, *ibid.* **360**, 29 (1992).
2. D. R. MacAyeal, *Nature* **359**, 29 (1992).
3. R. A. Bindschadler and T. A. Scambos, *Science* **252**, 242 (1991); see also T. A. Scambos and R. A. Bindschadler, *Eos* **73**, 182 (1992); T. A. Scambos *et al., Remote Sensing Environ.* **42**, 117 (1993).
4. R. H. Thomas, *J. Glaciol.* **24**, 167 (1979).
5. C. R. Bentley, *J. Geophys. Res.* **92**, 8843 (1987); I. M. Whillans, J. Bolzan, S. Shabtaie, *J. Geophys. Res.* **92**, 8895 (1987).
6. T. J. Hughes, *Rev. Geophys. Space Phys.* **15**, 44 (1977); J. Weertman and G. E. Birchfield, *Ann. Glaciol.* **3**, 316 (1982); C. S. Lingle and T. J. Brown, in *Dynamics of the West Antarctic Ice Sheet*, C. J. van der Veen and J. Oerlemans, Eds. (Reidel, Norwell, MA, 1987), p. 279; C. J. van der Veen, *ibid.*, p. 8.
7. R. B. Alley *et al., J. Glaciol.* **35**, 130 (1989); H. Engelhardt, N. Humphrey, B. Kamb, M. Fahnestock, *Science* **248**, 57 (1990); R. B. Alley, *Episodes* **13**, 235 (1990); B. Kamb, *J. Geophys. Res.* **96**, 16585 (1991).
8. The basic SRI method, but directed toward the detection of vertical displacements, was introduced by A. K. Gabriel, R. M. Goldstein, and H. A. Zebker [*J. Geophys. Res.* **94**, 9183 (1989)]; a version of the method for measuring horizontal flow in ocean currents was described by R. M. Goldstein and H. A. Zebker [*Nature* **328**, 707 (1987)] and by R. M. Goldstein, T. P. Barnett and H. A. Zebker [*Science* **246**, 1282 (1989)].
9. The SRI method was recently applied to the detection of ground displacement in an earthquake by D. Massonnet *et al.* [*Nature* **364**, 138 (1993)].
10. Theoretically, the two satellite locations must not be farther apart than about 100 m. These locations are occupied by the satellite at different times, in our case 6 days apart, on different orbital passes.
11. R. E. Crippen, *Episodes* **15**, 56 (1992).
12. As calculated from the radar return, the SAR images, called "single-look complex images" by ESA, contain both amplitude and phase information, given for each pixel in the form of a complex number. For a given positioning of the first image in relation to the second, starting from an approximate registry based on spacecraft orbit and image parameters, one compares the phase at each pixel in a test square (16 pixels by 16 pixels) in the first image with the phase at the corresponding pixel in the second, and the phase difference is coherently averaged over the square. This is done by a discrete two-dimensional Fourier transform of the complex numbers, which gives a correlation measure. This procedure is repeated with the second image shifted by a certain number of pixels relative to the first; 81 relative shifts, corresponding to shifts to pixels in a 9 by 9 square, are tested in this way. If a distinct maximum in the correlation measure is found within the 9 by 9 square, an interference-fringe pattern is indicated, and the maximum point is the local registry position for the two images. The procedure is repeated for a number of 16 by 16 squares distributed across the image. In the calculation of the interferograms, the registry position is taken to vary across the image in accordance with the smoothed results of the above registry search, allowing also for a discontinuity in registry position between the ice stream and the area outside of the ice stream. The variation is slight, one pixel spacing or less, but it has a significant effect on fringe quality.
13. Each original high-resolution image data set supplied by ESA consists of a 2,500 by 12,288 array of complex numbers giving pixel amplitude and phase, 2,500 rows in the range direction (bottom to top in Fig. 1), and 12,288 in the cross-range direction (right to left). We averaged the numbers by groups of 4 in the range direction and by groups of 12 in the cross-range direction, condensing the data set to a 625 by 1024 array, in which phase noise is greatly decreased by the averaging. Each data set covers half of the complete radar image; the near-range and far-range halves are combined to form the full interferogram. For Fig. 1, the pixel size on the ground is 80 m (on average) in range by 48 m in cross-range, and the dimensions of the area imaged is 100 km in range by 49 km in cross range, as shown by the *x* and *y* coordinate scales.
14. C. S. M. Doake *et al., J. Geophys. Res.* **92**, 8951 (1987).
15. R. M. Frolich *et al., Ann. Glaciol.* **12**, 51 (1989); especially figures 6 and 7.
16. S. N. Stephenson and C. S. M. Doake, *ibid.* **3**, 295 (1982).
17. S. N. Stephenson, *ibid.* **5**, 165 (1984).
18. U.S. Geological Survey and British Antarctic Survey, Satellite Image Map of Rutford Ice Stream, Antarctica (1:250,000) (1989).
19. The value $\psi \approx 24°$ agrees approximately with ground-based observations on line D of (*15*), but downstream from this line, considerably lower ψ values are found (down to $\psi \approx 7°$).
20. The bedrock of the Flowers Hills should, in principle, provide reference points of zero velocity, but the fringe pattern within the hills is so complicated that we cannot pick a zero-velocity fringe. For this reason, we take the reference point on ice at the edge of the hills. An alternative method for identification of the zero-velocity fringe makes use

of the curving flow of the Minnesota Glacier (Fig. 1). Where the flow traces are aligned along the *y* direction, the flow is perpendicular to the radar beam and the line-of-sight velocity component is zero. This criterion, applied to the flow traces and fringes near (69, 21), selects a zero-velocity fringe that differs by about 2 fringes from the one chosen at (26, 3).

21. In relation to the data averaging and condensing procedure described in (*13*), a smaller pixel size (16 m by 20 m) was obtained by averaging only in groups of four original pixels in the cross-range direction and doing no averaging in the range direction.
22. This is probably because interference cannot be obtained when the local rotation or rotational shear exceeds a certain limit. The shear is near the limit in Fig. 2 and exceeds it where the marginal zones are narrower. A similar limit was encountered in an SRI image of the Landers earthquake area (*9*): The fringes disappeared in a zone near the fault, where the shear strain was greatest. The rotation limit is when the *x* or *y* gradient of the line-of-sight displacement field is so large that each pixel contains a range of line-of-sight displacements spanning half a wavelength. The limit can be reduced with a reduction of the pixel size, as in Fig. 2. With a shorter time interval between SAR images (3 days in the case of ERS-1), the amount of rotation attributable to the shear flow of ice can be reduced in an effort to get below the limit.
23. A. M. Smith, *J. Glaciol.* **37**, 51 (1991).
24. This calculation was kindly done by C. S. M. Doake (personal communication).
25. Choice of the grounding line at coordinate 128 km is appropriate because $d\Delta z/dx = 0$ there on the observed curve (Fig. 3), which is what the model (*23*) assumes at $x = 0$. Because the model has $\Delta z = 0$ there, the uplift values on the calculated (dotted) curve are obtained by adding $\Delta z(x)$ from Eq. 1 to the observed uplift value (−0.05 m) at 128 km.
26. Very close agreement is not expected because the model assumes a two-dimensional flexure geometry, whereas the actual geometry is decidedly three-dimensional, with a tongue of grounded ice surrounded on three sides by floating ice that participates in tidal flexure (Fig. 1B).
27. The indication of grounding-line retreat in Fig. 4 is dependent on how the solid and dashed curves are positioned in relation to the indicated latitude and longitude lines. For the solid curve, the interferogram (Fig. 1A) was rescaled to the scale of the satellite image map (*18*) on the basis of image parameters furnished by ESA, and a transparency of the interferogram was registered to the map by registering the ice stream margins and the Flowers Hills. The latitude and longitude lines from the map were then transferred to the interferogram, on which the grounding line was drawn on the basis of the fringe pattern. For the dashed curve, the longitude and latitude lines in fig. 2 of (*17*) were transferred to fig. 5 of (*17*) with, as a reference, the frame of fig. 5 that is shown in fig. 2; after rescaling, we could position the grounding line in fig. 5 of (*17*) in our Fig. 4 by registering the latitude and longitude lines. Besides the uncertainties involved in the above procedure, the comparison in our Fig. 4 is made further uncertain by problematical aspects of the ground-based determination of the grounding line, as indicated by comparison of the results of (*17*) and (*24*).
28. H. J. Zwally *et al.*, *Science* **246**, 1587 (1989); C. J. van der Veen, *Rev. Geophys.* **29**, 433 (1991); D. J. Wingham *et al.*, *Eos* **74**, 113 (1993).
29. Although displacement resolution in SRI (conservatively ~1 cm for horizontal displacements) is much finer than in SSI (~30 m or 4.5 m) (*31*), for the measurement of ice flow velocities this advantage is offset by a limitation on the time interval between the SAR images usable by SRI, which is the time over which a velocity is measured. A 6-day interval has given SRI interference, but 12-day or longer intervals have not. In SSI, by contrast, optical images taken 2 years apart were usable in velocity determination (*3*). The reason for the limitation on SRI is that ongoing or occasional changes in the scattering surface caused by snow ablation or accumulation at the radar wavelength scale become extensive enough in about a week's time to destroy the detailed phase coherence between the two images on which the interference depends (*32*). In SSI, on the other hand, the changes have to be substantial on the pixel scale (~30 m) before velocity measurement is prevented. This tends to occur first in the marginal shear zones (*3*). The result of the above tradeoffs is a velocity resolution of about 0.6 m year^{-1} for SRI and about 2.3 m year^{-1} for SSI (*3*). For a shorter time interval between images, the velocity resolution will be correspondingly poorer.
30. An important element of glacier flow mechanics to which SRI and SSI data can readily make a contribution, because it requires only relative rather than absolute velocities, is analysis of the strain-rate field of the ice; C. J. van der Veen and I. M. Whillans, *J. Glaciol.* **35**, 53 (1989); *ibid.* **36**, 324 (1990).
31. The figure ~30 m represents pixel-scale resolution. Bindschadler and Scambos (*3*) achieved subpixel resolution (±4.5 m) by a cross-correlation method, and Crippen (*11*) cites examples of 0.05-pixel precision in sequential imaging applied to tectonic deformation.
32. In the recent report of SRI applied to ground displacement in the Landers earthquake (*9*), there is an interferogram from two images taken 105 days apart, which suggests that coherence-destroying changes of the ground surface in that area accumulate much more slowly than they do in the area of the Rutford Ice Stream.
33. The additional limitation of SRI to detection of motion only in the line-of-sight direction of the radar beam means that only one component of the horizontal flow can be directly measured from an image pair, whereas SSI obtains the full horizontal velocity. The limitation on SRI can be circumvented wherever the direction of the velocity vector is established by flow traces, as in Minnesota Glacier and the adjacent ice stream, or wherever the vector can reasonably be assumed parallel to a nearby ice stream margin. The limitation could also be overcome by a second interferogram with a roughly perpendicular line of sight, but this may or may not be obtainable, depending on the orbital and operational features of the satellite. However, because the ice stream motions and the motion sensitivity of SRI are so large, the measurement of one velocity component within, say, 60° of the flow direction would be sufficient for the monitoring of ice stream flow changes.
34. The repeatability is given as ~0.25 m by R. A. Bindschadler, H. J. Zwally, J. A. Major, and A. C. Brenner [*NASA Spec. Publ. SP-503* (National Aeronautics and Space Administration, Washington, DC, 1989)].
35. D. D. Blankenship, R. E. Bell, V. A. Childers, S. M. Hodge, *Eos* **73**, 129 (1992).
36. R. A. Massom, *Satellite Remote Sensing of Polar Regions* (Belhaven, London, 1991); see also R. M. Thomas, "Satellite Remote Sensing for Ice Sheet Research," *NASA Tech. Memo. 86233* (National Aeronautics and Space Administration, Washington, DC, 1985).
37. National Research Council Ad Hoc Committee on the Relation between Land Ice and Sea Level, *Glaciers, Ice Sheets, and Sea Level: Effect of a CO_2-Induced Climatic Change* (National Academy Press, Washington, DC, 1985); R. A. Warrick and J. Oerlemans, in *Climate Change: The IPCC Scientific Assessment*, J. T. Houghton, G. J. Jenkins, J. J. Ephraums, Eds. (Cambridge Univ. Press, Cambridge, 1990); R. A. Bindschadler, Ed., "West Antarctic Ice Sheet Initiative," *NASA Conf. Publ. 3115* (National Aeronautics and Space Administration, Washington, DC, 1991).
38. Research carried out in part by the Jet Propulsion Laboratory, California Institute of Technology, under a contract with the National Aeronautics and Space Administration. We thank ESA for making the SAR images available.

Greenland Ice Sheet Surface Properties and Ice Dynamics from ERS-1 SAR Imagery

Mark Fahnestock, Robert Bindschadler, Ron Kwok, Ken Jezek

C-band synthetic aperture radar (SAR) imagery from the European Space Agency's ERS-1 satellite reveals the basic zonation of the surface of the Greenland Ice Sheet. The zones have backscatter signatures related to the structure of the snowpack, which varies with the balance of accumulation and melt at various elevations. The boundaries of zones can be accurately located with the use of this high-resolution imagery. The images also reveal a large flow feature in northeast Greenland that is similar to ice streams in Antarctica and may play a major role in the discharge of ice from the ice sheet.

Understanding the current state of balance of ice sheets requires monitoring their mass exchange processes. An ice sheet's mass balance (*1*) primarily depends on snowfall, loss of mass due to surface melting and subsequent runoff, and the calving of icebergs from outlet glaciers which reach the sea. Measurement of the mass balance of an ice sheet is not simple. Changes in the margins of the ice sheet reflect a complex integration of fluctuating input, internal flow, and discharge processes that operate at different characteristic time scales. While it is not easy to measure directly a small change in the geometry of an entire ice sheet, it is

M. Fahnestock and R. Bindschadler are at the National Aeronautics and Space Administration Goddard Space Flight Center (NASA/GSFC), Greenbelt, MD 20771. R. Kwok is with the Jet Propulsion Laboratory, California Institute of Technology, Pasadena, CA 91109. K. Jezek is with the Byrd Polar Research Center, Ohio State University, Columbus, OH 43210.